Korean J. Chem. Eng., **24**(6), 1031-1036 (2007)

Photocatalytic activity of nitrogen-substituted TiO_2 deposited with Pt and Ru

Jaekyung Yoon, Sanghyun Bae*, Eunjung Shim and Hyunku Joo†**

Greenhouse Gas Research Center, Fossil Energy & Environment Research Department, Korea Institute of Energy Research, 71-2 Jang-dong, Yuseong-gu, Daejeon 305-343, Korea
*Department of Environment Engineering, Yonsei University, Wonju, Gangwon-do 220-710, Korea
**Department of Chemistry, Chungnam National University, 220 Gung-dong, Yuseong-gu, Daejeon 305-764, Korea
(*Received 6 March 2007 • accepted 30 April 2007*)

Abstract−In this work, Pt- and Ru-deposited, nitrogen-substituted TiO_2 were prepared and characterized by the discoloration of MB and H_2 evolution. The characteristics were evaluated in terms of methylene blue (MB) discoloration, open circuit voltage (OCV), photocurrent (I_{ph}), and hydrogen production. First, the Pt-deposited TiON revealed comparable activity in MB discoloration, while both TiONs resulted in somewhat less activity than P25. Second, an external bias was systematically applied to electrodes made of the prepared samples, resulting in –0.41~0.51 OCV, –400~400 μA and noticeable hydrogen evolution above 300 μA in absolute value when a bias of –1.5~1.5 V was applied to the working electrode of P25. The electrolyte and light intensity affected the light-responsive characteristics of the photocatalysts, confirming the relationship between OCV, I_{ph} and H_2 and that metal deposition slightly inhibited the I_{ph} and H_2 evolution while Ru-deposited TiON did not degrade MB effectively.

Key words: Photocatalyst, Nitrogen-doped, Metal Deposition, Photocurrent, Methylene Blue

INTRODUCTION

Environmental remediation and hydrogen evolution using a photocatalyst and/or photocatalytic system have been the subject of international research for a couple of decades [1,2]. With the tremendous amount of research performed on the surface properties, particle size, crystal phase and surface defects of various photocatalysts [3], recent studies on the preparation and efficiency enhancement of visible light-activated photocatalysts have attracted much attention [4,5]. Besides, the photocatalytic reaction may be drastically promoted, mostly due to the formation of Schottky barrier, or inhibited, mainly as charge recombination centers, by doping a photocatalyst with a certain kind of metal. In most cases, however, the doped metal acts as a catalyst for a reductive reaction such as hydrogen evolution [6]. Li et al. demonstrated that Pt-TiO_2 catalyst could also be sensitized by visible light and had optimal content of 0.75 wt% for the best performance of methylene blue (MB) degradation [7]. Platinum has been studied as one of the most active metals capable of facilitating electron capture for photocatalytic enhancement, which can produce the highest Schottky barrier [8]. Unlike Pt, Ru has found only relatively limited use. Ohno et al. studied Ru-doped TiO_2 powder for photocatalytic oxidation of water by visible light, where its oxidation power was examined, and Sasirekha et al. investigated the photocatalytic performance for the reduction of carbon dioxide (optimum 0.5 wt%) [9,10]. They also reported that the metal deposition itself absorbed visible light and that variation in the metallizing method could alter the activity or reaction mechanism. To the best of the authors' knowledge, little research has investigated the metal doping on anion-substituted TiO_2, compared to the extensive study on pure TiO_2. Therefore, in the present study, two metals (Pt and Ru) are photodeposited on commercial P25 and home-made nitrogen-substituted TiO_2 in order to examine the photocatalytic discoloration of MB and evolution of hydrogen with photocurrent (I_{ph}) and open circuit voltage (OCV) measurement. The electrochemical approach is useful for photocatalysis, but when particles are deposited on the metal or conductive material, the total resistivity of the photocatalyst must be minimized. The scope of this work does not include the method of immobilization, which is obviously important for practical applications. The immobilization or 'one-body' photocatalytic material by anodizing of metal substrate will be dealt with in a subsequent article.

EXPERIMENTAL PROCEDURE

All chemicals were used without further purification. MB (Aldrich 85%) was used as the probe compound for measuring activity. P25 TiO_2 powder was generously provided by Degussa. In this work, visible, light-activated, nitrogen-substituted titanium oxide (TiON) was prepared by sol-gel (TTIP, HCl, ethanol) with NH_3 aqueous solution (28% in H_2O, Junsei Chemical) followed by air drying and heat treatment at various temperatures. The detailed experimental procedure has been described in a previous study [11]. Pt and Ru were photodeposited on TiON powders (Pt- or Ru-TiON hereafter) for 5 hrs by using H_2PtCl_6 and $RuCl_4$, respectively, with methanol as a hole scavenger, followed by filtering and drying at 80 °C.

The light source was a 1,000 W xenon lamp (Oriel, USA), which was filtered through a 10-cm IR water filter and a cut-on filter (LG-450-S, Oriel). Crystal phase and size were determined by X-ray diffraction (XRD, Miniflex, Rigaku; k=0.89, ramda=0.15418 for CuKα X-ray, 30 kV, 15 mA), and the change in absorbance of characteristic peaks of MB was measured with UV/Vis (Perkin Elmer rambda2) during the discoloration of MB in slurry reactor (reactor volume 100 mL, initial concentration of MB 100 ppm, and 0.2 g of powered

†To whom correspondence should be addressed.
E-mail: hkjoo@kier.re.kr

photocatalyst). A computer-controlled potentiostat (FSA2, PHE200, GAMRY) was employed to control the bias and measure the OCV and Iph. The reference (Ag/AgCl) and counter (Pt wire) electrodes were used with a salt-bridge in the middle of two compartments. The surface conditions of the prepared samples were determined by X-ray photoelectron spectroscopy (XPS, Escalab 200R, VG Scientific. Co.) using Al Ká radiation. The X-ray source was operated at 300 W and 20 mA. The vacuum of the analysis chamber was lower than 5×10^{-10} torr during analysis. For narrow scans, the step size used was 0.1 eV. The standard reference energy used for the experimental calibration was the Au_{4f} peak at 84.0 eV. All the binding energies were referenced to the C_{1s} peak at 284.8 eV of the adventitious surface hydrocarbons, which are invariably present on the film surface. All spectra were fitted with a linear background to an 80% Gaussian/20% Lorentzian peak shape.

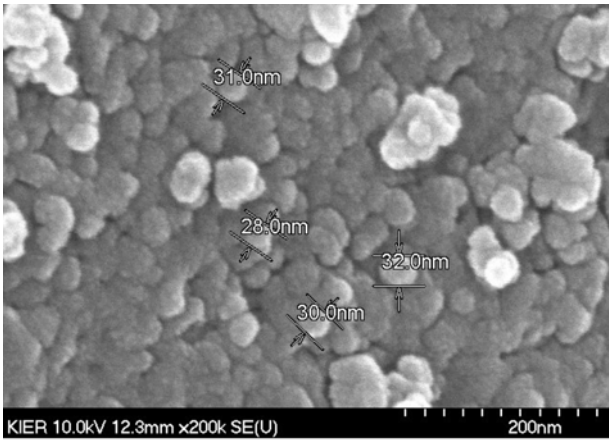

(a) Pt/TiON (photoreduced for 1hr)

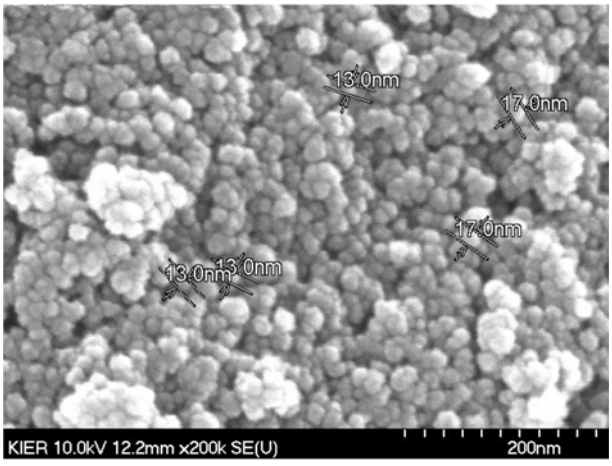

(b) Ru/TiON (photoreduced for 1hr)

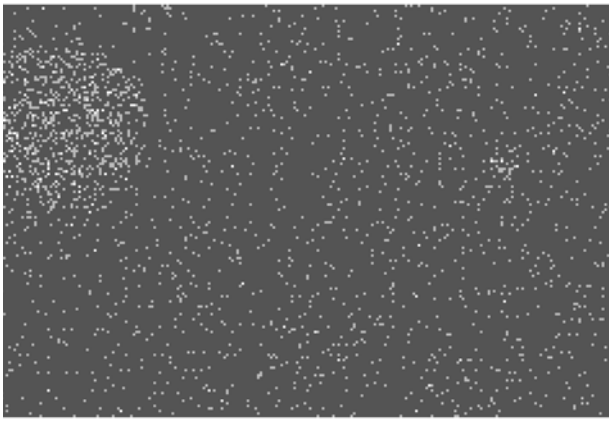

(c) map of Ru for sample (b)

Fig. 1. SEM images of (a) Pt- and (b) Ru-deposited TiON and map of Ru for (b).

RESULTS AND DISCUSSION

The SEM images of metal-deposited TiONs are shown in Fig. 1. The dispersion of Ru is also shown in the image of the Ru/TiON constituents. The TEM images of P25, nitrogen-substituted TiO_2 ("TiON" hereafter), Pt- and Ru-deposited TiON clearly identified the lattice structure and the presence of the deposited metals, while a morphological difference was observed between two catalysts (Fig. 2).

XRD analysis of Pt- and Ru-TiON (Fig. 3) indicated a main characteristic anatase peak at 2θ=25.3 for both samples. Average crystallite sizes calculated from the broadening of the (101) plane XRD peak of the anatase phase were 25.4 nm for P25 and 9.8 nm for TiONs. The P25 crystallite size of 25.4 nm was consistent with that obtained from transmission electron microscopy (Fig. 2) and also available in the literature. The weight ratio of anatase (f_a) to rutile (f_r) of P25,

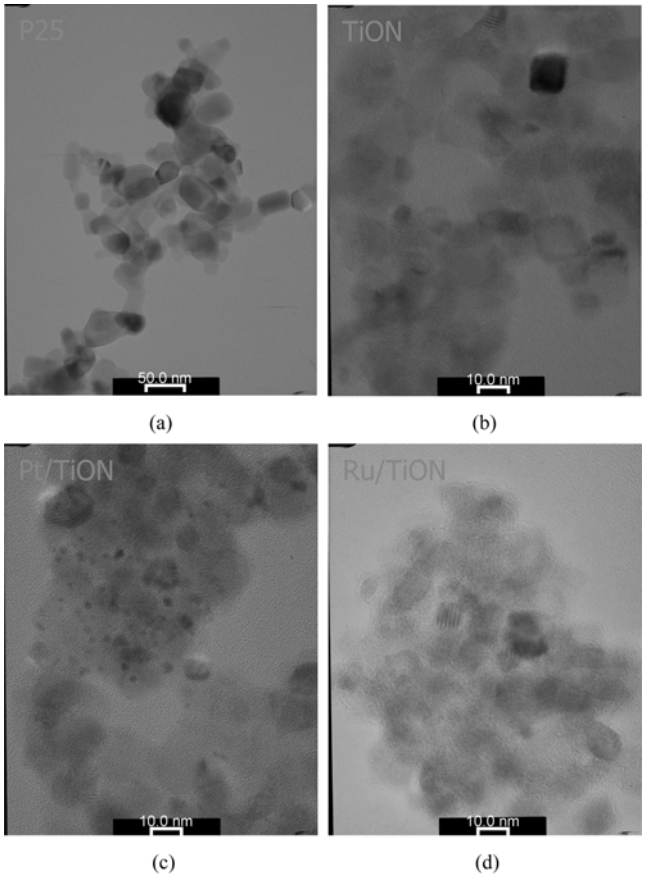

Fig. 2. TEM images of (a) P25, (b) TiON, (c) Pt/TiON and (d) Ru/TiON.

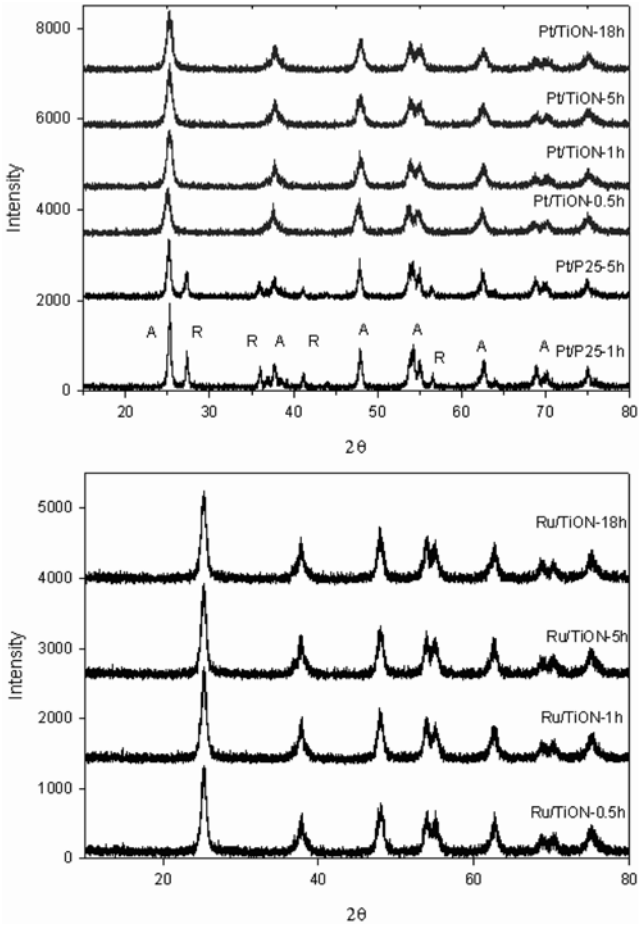

Fig. 3. XRD patterns of Pt (top) and Ru (bottom)-deposited TiON.

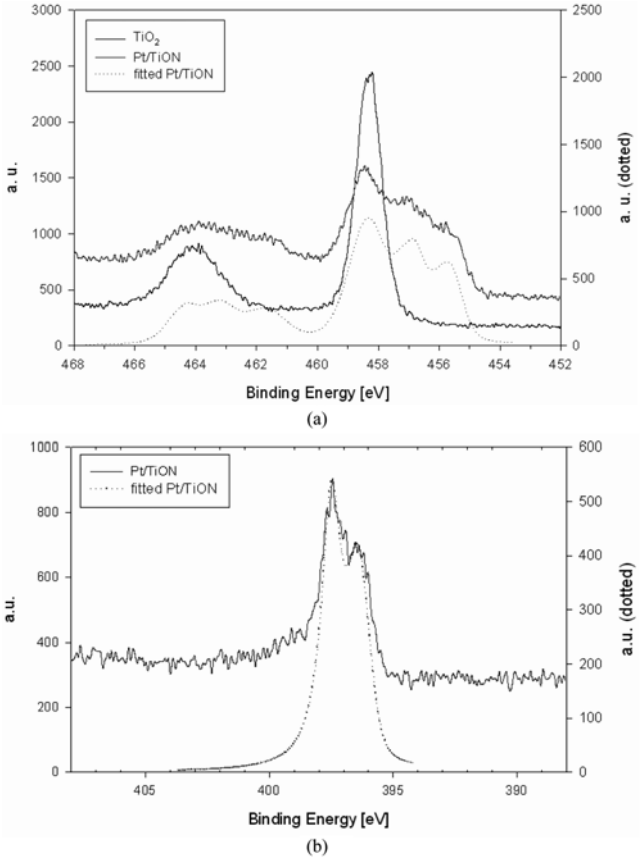

Fig. 4. XPS patterns of (a) Ti_{2p} and (b) N_{1s} of Pt/TiON.

calculated by Eqs. (1) and (2) to be 0.63 : 0.36, well matched the supplier's specifications. The calculated crystallite size of 9.8 nm for TiON was also in good agreement with that obtained from a high-resolution electron micrograph.

$$f_a=(1+1.26I_r/I_a)^{-1} \quad (1)$$

$$f_r=(1+0.8I_a/I_r)^{-1} \quad (2)$$

where I_a and I_r are XRD intensities of the 101 (2θ=25.3) and 110 (2θ=27.3) peaks, corresponding to 1,941 and 883, respectively. XRD showed that the crystal phase of TiON was anatase and that the deposition of metals seldom affected the crystal phase of TiON. The broader peaks of metal-deposited TiONs indicated lower crystallinity and smaller crystal size than those of P25. Energy dispersive X-ray analysis indicated Pt and Ru deposition rates of 0.53% and 0.56%, respectively, when photodeposited for 5 hr, which well matched the calculated values. In Fig. 4, XPS analysis clearly indicates a photoelectron peak for Ti 2p at a binding energy, E_b, of 458 eV, O 1s at 531 eV and C 1s at 284 eV [12]. The Ti 2p region was composed of two contributions corresponding to the different oxidation states of titanium: $\Delta E_b=E_b(Ti\ 2p_{1/2})-E_b(Ti\ 2p_{3/2})$ is always 5.7 eV, as previously reported in the literature [13]. The symmetric peaks of the corresponding doublet are shown situated at E_b (Ti $2p_{3/2}$)=529.8 eV and E_b (Ti $2p_{1/2}$)=531.5 eV, which is in agreement with the literature values [4,5,14]. XPS peak at 396 eV represents N 1s and is clearly observed in Fig. 4(b).

MB is a cationic dye molecule and has been known to be unreactive in the TiO_2 system at pH=3 for two reasons: the weaker thermodynamic driving force for the electron injection from the excited state of MB (MB*) to conduction band (CB) of TiO_2, and the electrostatic repulsion between MB^+ and the positively charged TiO_2 surface [15]. In this study, the metal-deposited TiON system was located at pH 5-6, confirming the neutral surface charge of the catalyst and the minimization of the repulsion force. The discoloration of MB can be induced by two different mechanisms: the oxidative destruction of the chromophoric aromatic rings and the reductive conversion to its colorless form. In the absence of any characteristic peak at 256 nm for the latter, the former mechanism (peak at 662 nm) appeared to be applied in our study. Fig. 5 shows the time-coursed profiles of MB discoloration with the Pt- and Ru-deposited TiONs along with P25 as a reference. Unlike the Ru-deposited TiON, the Pt-deposited TiON revealed comparable activity in MB discoloration, while both TiONs resulted in somewhat less activity than P25. Crystallinity is known to be essential in photocatalysis and the lower crystallinity of TiONs seemed to cause lower activity in MB discoloration in Fig. 5. Furthermore, the band position of TiONs might be another reason. The Langmuir-Hinshelwood kinetics (3), generally applied in photocatalysis, indicates that a relatively high concentration of a probe material converts the equation to zero order kinetics, evidenced in our study by the simple experiment of varying the amount of photocatalyst with a fixed initial concentration of MB (100 ppm) in order to change the time-coursed profiles of

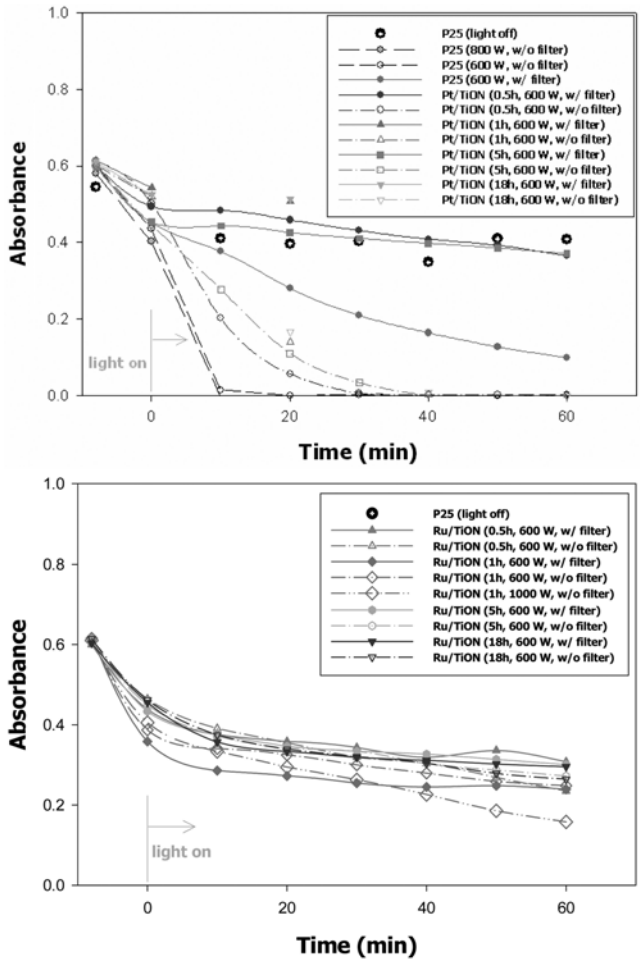

Fig. 5. Photocatalytic decolorization of methylene blue with metal-deposited TiON (top: Pt/TiON, bottom: Ru/TiON, 100 ml of methylene blue (100 ppm), 0.2 g of photocatalyst).

MB discoloration from first order to zero order with decreasing injection amount.

$$r = k\frac{KC}{1+KC} \tag{3}$$

The optical absorption spectra of TiONs were investigated previously by using UV/Vis. Visible light section at wavelength below 550 nm was absorbed by TiONs, but not by P25. This absorbance of TiONs peaked at the heat treatment of 400 °C among the experimented calcinations temperatures of 200, 300, 400, 500, and 600 °C. Besides visible light absorption, photocatalytic activity is essential for the application of TiONs. A commercial UV-A lamp and solar simulator with 450 nm cutoff filter were used for this purpose in terms of the photodegradation of isopropyl alcohol (IPA). Acetone evolution as a function of UV-A irradiation time revealed a slightly inferior evolution rate with TiONs compared to that with P25 (approximately 75%). Meanwhile, under visible light irradiation the

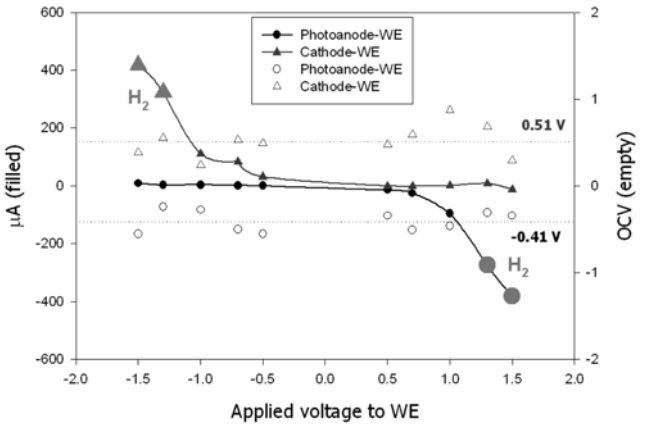

Fig. 7. Comparison of results for OCV, I_{ph} and hydrogen evolution.

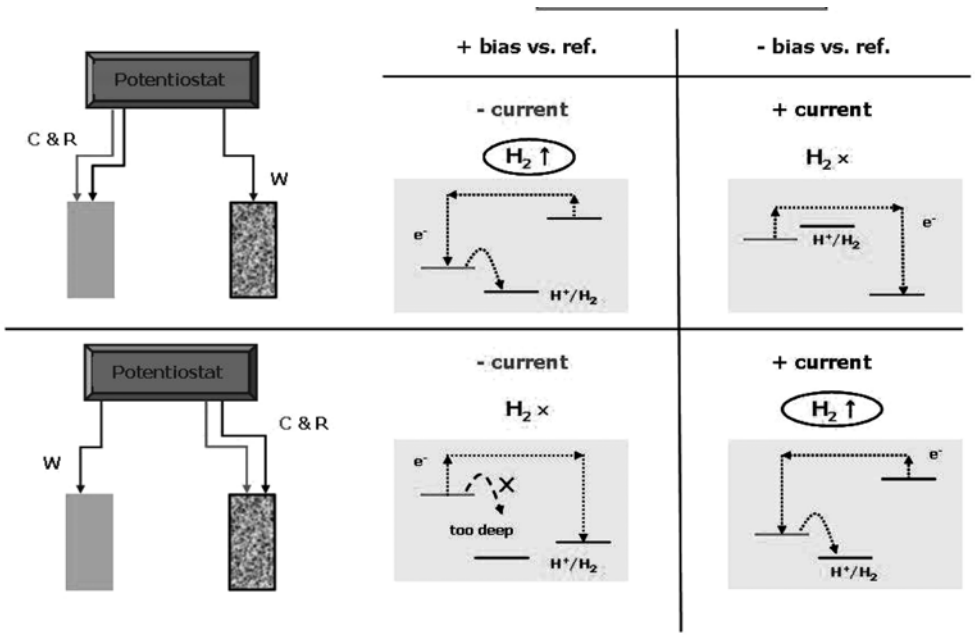

Fig. 6. Schematic diagram of external bias application and postulated energetic mechanism (W: working electrode, C: counter electrode, R: reference electrode).

acetone evolution rate for TiONs was noticeably higher than that of P25.

Figs. 6 and 7 present that experimental setup with P25 for electrochemical measurement and summarize the comparative results for OCV, I_{ph} and hydrogen evolution. The working electrode (WE) was placed on either the photoanode or the Pt cathode and the reference electrode (PE) was Ag/AgCl in saturated KCl. Then, external bias was applied onto WE by potentiostat from −1.5 to +1.5 V. Negative bias onto WE or positive bias onto the counter electrode (CE) produced a positive current indicating an electron flow from the photoanode to the cathode and hydrogen evolution in the cathode compartment. Otherwise, a negative current was indicated without any hydrogen evolution. A possible energetic level scheme is indicated in Fig. 6. OCV and generated current values were –0.41~0.51 V and −400~400 μA, respectively. Noticeable hydrogen evolution was identified at a current above 300 μA when 1.3 V bias in absolute value was applied to the electrode. The results of a preliminary study applied with metal-deposited TiONs are summarized in Tables 1 and 2. The electrolyte effect confirmed that Na_2S and Na_2SO_3 enhanced hydrogen evolution irrespective of the photocatalysts used. Sulfide and sulfite ion have similar standard reduction potentials of −0.476 and −0.571, respectively, indicating the strong potential for electrons to be transferred to the valence band of the photocatalysts. Ru-doped P25 showed the highest rate of hydrogen evolution, but metal doping did not evidence any consistent effect for TiONs. Light intensity also differentiated the rate of hydrogen evolution. The resultant trends of OCV and I_{ph} were fairly well matched with that of hydrogen evolution in view of the greater negativity of OCV and I_{ph} for the electrolytes with Na_2S and Na_2SO_3. Generally speaking, any accumulation of electrons in a photocatalyst shifts the Fermi level to a more negative potential, thereby leading to a more negative OCV. It was also clearly indicated that the OCVs of the system (dark) differed from each other (OCV represents the difference between the Fermi level and the reduction potential of the redox couple [16]) and that the application of light reduced the band bending and increased OCV. However, the effect of photocatalyst within an electrolyte was difficult to implement.

CONCLUSION

The electrolyte and light intensity affected the light-responsive characteristics of photocatalysts and these characteristics were closely related with the rate of hydrogen evolution. Recently, the photoelectrochemical system has dominated the photocatalytic system in

Table 1. Evolved hydrogen quantity (μmol) after 4 hr of irradiation

Catalyst	Loaded materials	Na_2CO_3 (0.1 M)		Na_2CO_3 (2.0 M)		Na_2S (0.1 M)		Na_2SO_3 (2.0 M)	
		1,000 W	500 W	1,000 W	500 W	1 000W	500 W	1,000 W	500 W
P-25	-	0	0	0/1.459	0	6.27	3.82	3.88	-
	Pt (0.5 wt%)	0	0	0/0	0	6.04	-	2.85	-
	Ru (0.5 wt%)	0	0	0	0	8.49	-	4.25	-
TiON 400	-	0	0	1.707	-	4.76	-	4.02	-
	Pt (0.5 wt%)	0	0	0.098	0	3.3395	-	3.66	-
	Ru (0.5 wt%)	0	0	0.254	-	5.61	-	3.219	-

Table 2. OCV and I_{ph} with various combinations of photocatalysts and electrolytes

Catalyst	Loaded materials	Na_2CO_3 0.1 M				Na_2CO_3 2.0 M			
		Lamp-off		Lamp-on		Lamp-off		Lamp-on	
		OCV (mV)	I_{ph} (μA)	OCV (mV)	I_{ph} (μA)	OCV (mV)	I_{ph} (μA)	OCV (mV)	I_{ph} (μA)
P-25	-	−224	1.1	−612	−28	−194	1.3	−956	−22
	Pt (0.5 wt%)	−166	1	−620	−20	−171	1.2	−650	−13.5
	Ru (0.5 wt%)	−190	1.2	−588	−16	−202	1.2	−530	−2
TiON 400	-	−158	1.1	−935	−60	−130	1.2	−1,050	−200
	Pt (0.5 wt%)	−148	1	−835	−66	−125	1.2	−980	−175
	Ru (0.5 wt%)	−152	1.2	−796	−60	−109	1.1	−940	−198
Catalyst	Loaded materials	Na_2S 0.1 M				Na_2SO_3 2.0 M			
		Lamp-off		Lamp-on		Lamp-off		Lamp-on	
		OCV (mV)	I_{ph} (μA)	OCV (mV)	I_{ph} (μA)	OCV (mV)	I_{ph} (μA)	OCV (mV)	I_{ph} (μA)
P-25	-	−606	13.5	−1,260	−126	−125	1.1	−1,120	−270
	Pt (0.5 wt%)	−596	14	−1,150	−97	−130	1.2	−1,080	−250
	Ru (0.5 wt%)	−532	13	−1,120	−110	−150	1.1	−1,030	−222
TiON 400	-	−576	14	−1,200	−170	−109	1.2	−1,100	−268
	Pt (0.5 wt%)	−574	14	−1,140	−143	−120	1.1	−1,050	−235
	Ru (0.5 wt%)	−570	14	−1,180	−115	−120	1.2	−1,020	−270

the research on solar hydrogen. This necessitates the use of an electrode and further research to define the preliminary criteria of its efficiency. The process examined in the present study for the investigation of this aforementioned requirement can be updated to a specific research field on the photo/biocatalytic hydrogen system. Recently, a self-assembled photoanode has been prepared and used for hydrogen evolution, with a production rate of 45 μmol/(hr×cm^2), which corresponds to an STH (solar-to-hydrogen basis) rate of approximately 3%. The continuing upgrade of photoanodes necessitates their electrochemical testing, as well as hydrogen evolution, under various reaction conditions.

ACKNOWLEDGMENTS

This research was performed for the Hydrogen R&D Center, one of the 21st Century Frontier R&D Programs, funded by the Ministry of Science and Technology of Korea.

REFERENCES

1. D. F. Ollis and H. Al-Ekabi, *Photocatalytic purification and treatment of water and air*, Elsevier, Amsterdam (1993).
2. N. Serpone and E. Pelizzetti, *Photocatalysis: Fundamentals and applications*, John Wiley & Sons, New York (1989).
3. S. Sakthivel, M. V. Shankar, M. Palanichamy, B. Arabindoo, D. W. Bahnemann and V. Murugesan, *Water Research*, **38**, 3001 (2004).
4. T. Ihara, M. Miyoshi, Y. Iriyama, O. Matsumoto and S. Sugihara, *Applied Catalysis B: Environmental*, **42**(4), 403 (2003).
5. R. Ashai, T. Morikawa, T. Ohwaki, K. Aoki and Y. Taga, *Science*, **293**, 269 (2001).
6. J. Sha and S. Fumihide, *Chemical Engineering Journal*, **97**, 203 (2004).
7. F. B. Li and X. Z. Li, *Chemosphere*, **48**, 1103 (2002).
8. A. V. Vorontsov, I. V. Stoyanova, D. V. Kozlov, V. I. Simagina and E. N. Savinov, *J. of Catalysis*, **189**, 360 (2000).
9. T. Ohno, F. Tanigawa, K. Fujihara, S. Izumi and M. Matsumura, *J. of Photochem. & Photobiol A: Chem.*, **127**, 107 (1999).
10. N. Sasirekha, S. J. Sardhar and K. Shanthi, *Applied Catalysis B: Environmental*, **62**, 169 (2006).
11. H. Shin, H. Joo, J. Park and C. H. Lee, *Materials Science Forum*, **449**, 1257 (2004).
12. D. Briggs and M. P. Seah, *Practical surface analysis: by auger and X-ray photoelectron spectroscopy*, John Wiley & Sons, New York (1983).
13. C. D. Wagner, W. M. Riggs, L. E. Davis, J. F. Moulders and G. E. Mullenberg, *Handbook of X-ray photoelectron spectroscopy*, Perkin-Elmer Corporation, Eden Prairie, MN (1979).
14. J. Yu, X. Zhao and Q. Zhao, *Materials Chem. & Phys.*, **69**, 25 (2001).
15. H. Park and W. Choi, *J. Phys. Chem. B*, **109**, 11667 (2005).
16. C. He, X. Li, Y. Xiong, X. Zhu and S. Liu, *Chemosphere*, **58**, 381 (2005).